Online Monitoring of Interturn Short Circuit Current in PMSMs

1st Lukas Zezula
CEITEC, Department of Control and Instrumentation
Brno University of Technology
Brno, Czech Republic
lukas.zezula@ceitec.vutbr.cz

2nd Petr Blaha
Central European Institute of Technology (CEITEC)
Brno University of Technology
Brno, Czech Republic
petr.blaha@ceitec.vutbr.cz

Abstract—This paper extends the previously published parameter estimation-based approach to interturn short circuit diagnostics in permanent magnet synchronous motors by real-time monitoring of hidden machine states after fault occurrence. The designed monitoring method relies on an adaptive formulation of the Kalman filter, which assumes interdependence between measurement and process noise variables. A variable forgetting factor not only mitigates the impact of the process model uncertainty but also facilitates the simultaneous operation of the monitoring algorithm and fault indicator estimation. Furthermore, contributions of fault current and healthy machine model to stationary reference frame currents are estimated from an advanced discrete-time motor description reflecting a stator winding arrangement inside a motor's case. The monitoring algorithm is validated in steady state, torque load transient, and velocity transient laboratory experiments with diverse fault severity values.

Index Terms—discrete-time systems, fault currents, fault diagnosis, Kalman filters, permanent magnet machines, short-circuit currents, state estimation.

I. INTRODUCTION

Currently, Permanent Magnet Synchronous Motors (PMSMs) are extensively used across diverse industrial and automotive applications where higher safety and availability requirements apply. Due to these requirements, modern electrical drives featuring PMSMs must ensure continuous operability at their standard or reduced capabilities even after fault occurrence. In this context, the risk of Interturn Short Circuits (ISCs), typically caused by thermal degradation between the coil turns in a stator winding of PMSMs, becomes a critical concern, as these faults can compromise both the

safety and availability requirements. The combination of low short circuit resistance and higher voltage, increased by the flux linkage of permanent magnets, produces a significant fault current. The heat generated by the high-value fault current then further degenerates the insulation material, and this self-heating circle might eventually lead to a motor's breakdown and potential fire [1]. Thus, rapid and reliable fault diagnostics and mitigation are required to prevent the described scenario. The modern fault mitigation algorithms [2] - [5] utilizing, for example, model predictive control strategies commonly require extended information about a shorted motor to function. The necessary characteristics include not only fault occurrence indication but also estimations of electrical parameters, fault severity, fault location, and hidden machine states that are not directly measured (e.g., current flowing through the short circuit).

The previous research [6] addressed ISCs detection, localization, and severity estimation based on the model comparison [7] and parameter estimation [8] algorithms cast in a decision-making framework. Through the Bayesian approach and specially designed discrete-time model [9] - [10], fault diagnostics functioned even in the velocity and torque load transient state. Furthermore, as the noise precision was learned with the estimated parameters, the designed algorithm proved robust to the system noise. This paper aims to extend the previously designed diagnostics by online monitoring of the hidden motor states, considering not only the fault current but also the contributions of a healthy motor model to the overall currents. For this purpose, Kalman filtering with the variable forgetting factor [11] was adopted.

Kalman filtering has previously shown effectiveness in fault detection [12] - [13], indicator estimation [14] - [15], and fault current monitoring [16]. As [16] discusses a topic related to this paper, we carefully examined the presented fault current monitoring method and identified the subsequent drawbacks:

1) The algorithm is built upon the simplified winding model, which assumes the whole stator winding is concentrated in one coil segment. As most PMSMs contain series, parallel, or series-parallel connected coil segments, the utilized model neglects actual inductive couplings and provides overrated fault current estimations [9].
2) The discrete-time equivalent of the specified model is

obtained using the forward Euler discretization method. As proved in [10], this method provides numerically unstable results considering a motor operating at higher velocities.

3) The estimation error of the extended Kalman filter utilized in [16] highly depends on the initialization of covariance matrices, which are adjusted using trial and error experiments. Considering drawbacks 1) and 2), the covariance of the process noise is most likely velocity-dependent, and provided adjustment might not be valid for additional operating points.

In this paper, we address all the problems mentioned above as the utilized model reflects the winding arrangement in a motor's case, the semi-analytical discrete-time equivalent is derived using the exact solution for linear time-varying systems, and the conventional Kalman filter is replaced by an adaptive variant designed to mitigate the process model uncertainty. Alternative approaches to fault current estimation are based, for example, on the second harmonic monitoring in reference voltages and feedback currents [17], proportional-integral estimator [18], moving horizon observer [19], or utilization of model predictive control technique [20]. Nevertheless, a drawback of these techniques is their limited functionality in the transient states.

The paper is organized as follows: Section II describes the utilized discrete-time model, Section III is dedicated to an overview of the adaptive Kalman filter [11] and incorporation of the designed hidden state monitoring to fault diagnostics [6], and Section IV demonstrates the laboratory experiment results.

II. DISCRETE-TIME MODEL

The utilized discrete-time model is calculated from the continuous-time description, which was derived in [9] as in

$$
\frac{\mathrm{d}}{\mathrm{d}t}\begin{bmatrix} i_{\alpha,h} \\ i_{\beta,h} \end{bmatrix} = -\frac{R_s}{L_s}\begin{bmatrix} i_{\alpha,h} \\ i_{\beta,h} \end{bmatrix} + \frac{1}{L_s}\begin{bmatrix} u_\alpha \\ u_\beta \end{bmatrix} + \frac{\omega_e\lambda_{pm}}{L_s}\begin{bmatrix} \sin(\theta_e) \\ -\cos(\theta_e) \end{bmatrix}
$$

$$
\frac{\mathrm{d}}{\mathrm{d}t}i_f = -\frac{R_f^*}{L_f}i_f + 3\frac{x_f}{n_s L_f}\begin{bmatrix} \cos\left(\frac{\phi}{2}\right) & -\sin\left(\frac{\phi}{2}\right) \end{bmatrix}\begin{bmatrix} u_\alpha \\ u_\beta \end{bmatrix}
$$

$$
R_f^* = (1 - 3n_p)R_s\frac{x_f^2}{n_s^2} + 3n_p R_s\frac{x_f}{n_s} + 3R_f
$$

$$
L_f = 2\frac{x_f^2 n_p(n_s - 1)}{n_s^2}L_s
$$

$$
\begin{bmatrix} i_\alpha \\ i_\beta \end{bmatrix} = \begin{bmatrix} i_{\alpha,h} \\ i_{\beta,h} \end{bmatrix} + \frac{2x_f}{3n_s}i_f\begin{bmatrix} \cos\left(\frac{\phi}{2}\right) \\ -\sin\left(\frac{\phi}{2}\right) \end{bmatrix} \tag{1}
$$

where i_α, i_β and u_α, u_β are the stationary reference frame currents and voltages; variables ω_e and θ_e denote electrical angular velocity and angle; and the electrical parameters R_s, L_s, and λ_{pm} stand for the stator resistance, inductance, and permanent magnet flux linkage, respectively. Parameters n_p and n_s are then related to the distribution of the stator winding inside a motor's case, where n_p represents the number of parallel-connected winding branches, and n_s is the number of coils in series in each branch as depicted in Fig. 1.
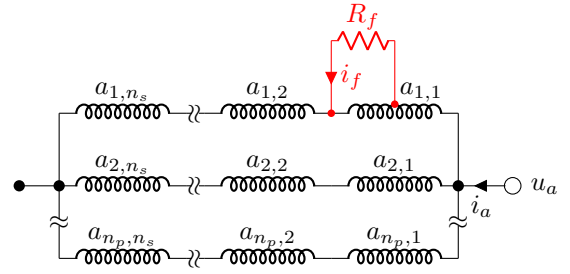

Fig. 1. The phase a winding under an interturn short circuit fault.

Parameters n_p and n_s can be obtained by examining the winding of a utilized PMSM. The fault-related characteristics i_f, x_f, R_f, and ϕ then denote the fault current flowing through ISC, fault severity quantifying the proportion of shorted turns to total turns within one coil segment, short circuit resistance, and fault location in terms of the angle of shorted phase ($\phi = \{0, 2\pi/3, -2\pi/3\}$ means that ISC is in phase $\{a, b, c\}$), respectively. Furthermore, as seen in (1), the resulting $\alpha - \beta$ currents are composed of the weighted fault current i_f and contributions $i_{\alpha,h}$ and $i_{\beta,h}$ generated by the model of a healthy motor (the first equation in (1)). These variables pose hidden states to be estimated using the Kalman filtering.

According to [6], parameters x_f and R_f cannot be separated from each other in the estimation procedure. Thus, fault severity is estimated as a converted value assuming zero short circuit resistance $x_f(R_f = 0\,\Omega)$. This conversion complicates fault current monitoring because it disables the distinction between a higher-value fault current flowing through a few shorted turns and a lower fault current flowing through more shorted turns, as they both have a comparable impact on the overall $\alpha - \beta$ currents (see the last equation in (1)). Therefore, we have decided to merge these fault-related characteristics into one hidden state to be tracked. We have

$$
\tilde{i}_f = x_f i_f
$$

$$
\frac{\mathrm{d}}{\mathrm{d}t}\tilde{i}_f = -\frac{R_f^*}{L_f}\tilde{i}_f + 3\frac{x_f^2}{n_s L_f}\begin{bmatrix} \cos\left(\frac{\phi}{2}\right) & -\sin\left(\frac{\phi}{2}\right) \end{bmatrix}
$$

$$
\begin{bmatrix} i_\alpha \\ i_\beta \end{bmatrix} = \begin{bmatrix} i_{\alpha,h} \\ i_{\beta,h} \end{bmatrix} + \frac{2}{3n_s}\tilde{i}_f\begin{bmatrix} \cos\left(\frac{\phi}{2}\right) \\ -\sin\left(\frac{\phi}{2}\right) \end{bmatrix}. \tag{2}
$$

In formulating the discrete-time model, it is crucial to make satisfactory approximations of the input voltages u_α, u_β and variables ω_e and θ_e to prevent solving a system of nonlinear differential equations. As the $\alpha - \beta$ inputs are linearly transformed from the stator voltages (abc) produced by inverter switching, width-modulated pulses are present even in the stator reference frame. Despite this, with adjusted current sampling effectively suppressing ripple, the modulation can be neglected, and the $\alpha - \beta$ voltages between the sampling intervals are expressed as follows:

$$
\begin{aligned}
u_\alpha(t) &= u_\alpha(k-1) & (k-1)T_s \leq t < kT_s \\
u_\beta(t) &= u_\beta(k-1) & (k-1)T_s \leq t < kT_s
\end{aligned} \tag{3}
$$

where k is the current step of the discrete-time system, T_s represents the sampling period, and t denotes the time. Since

only minor velocity changes occur in the sampling interval [10], ω_e can be approximated by a constant value $\omega_e(t) \approx \bar{\omega}_e$ as in

$$\bar{\omega}_e = \frac{\omega_e(k) + \omega_e(k-1)}{2} \qquad (k-1)T_s \leq t < kT_s. \qquad (4)$$

Approximation (4) then leads to the linear angle between the sampling intervals. We have

$$\theta_e(t) \approx \theta_e(k-1) + \big(t - (k-1)T_s\big)\bar{\omega}_e. \qquad (5)$$

Expression (5) is again valid only at $(k-1)T_s \leq t < kT_s$.

By using the approximations of electrical angular velocity and angle (4) and (5), system (1) can be discretized as a general linear time-invariant description [10], where the parts containing $\sin\big(\theta_e(t)\big)$ and $\cos\big(\theta_e(t)\big)$ (the first equation in (1)) are attributed to the vector of inputs. The resulting discrete-time model reads

$$\underbrace{\begin{bmatrix} i_{\alpha,h}(k) \\ i_{\beta,h}(k) \\ \tilde{i}_f(k) \end{bmatrix}}_{\mathbf{x}(k)} = \mathbf{A} \underbrace{\begin{bmatrix} i_{\alpha,h}(k-1) \\ i_{\beta,h}(k-1) \\ \tilde{i}_f(k-1) \end{bmatrix}}_{\mathbf{x}(k-1)} + \mathbf{B} \underbrace{\begin{bmatrix} u_{\alpha}(k-1) \\ u_{\beta}(k-1) \\ v_{\alpha}(k,k-1) \\ v_{\beta}(k,k-1) \end{bmatrix}}_{\mathbf{u}(k-1)} + w(k)$$

$$\underbrace{\begin{bmatrix} i_{\alpha}(k) \\ i_{\beta}(k) \end{bmatrix}}_{\mathbf{y}(k)} = \mathbf{C} \begin{bmatrix} i_{\alpha,h}(k) \\ i_{\beta,h}(k) \\ \tilde{i}_f(k) \end{bmatrix} + e(k) \qquad (6)$$

where $w(k) \in \mathbb{R}^3$ and $e(k) \in \mathbb{R}^2$ denote the process and measurement noises, constituting mutually dependent, zero-mean, normally distributed white noise sequences. The interdependence among the noises was defined in [11] as follows:

$$\varepsilon_{\{w,e\}} \left[\begin{bmatrix} w(k) \\ e(k) \end{bmatrix} \begin{bmatrix} w(k) \\ e(k) \end{bmatrix}^T \right] = \begin{bmatrix} \mathbf{Q} & \mathbf{S} \\ \mathbf{S}^T & \mathbf{R} \end{bmatrix}. \qquad (7)$$

In (7), upper index T refers to the transposition, expression $\varepsilon_{\{x\}}[f(x)]$ describes the expectation of a function $f(x)$ over x, and covariance matrices $\mathbf{Q}^{3\times3}$, $\mathbf{S}^{3\times2}$, and $\mathbf{R}^{2\times2}$ are assumed known. Matrices $\mathbf{A}$, $\mathbf{B}$, and $\mathbf{C}$ are then derived as in

$$\mathbf{A} = \begin{bmatrix} e^{-\frac{R_s}{L_s}T_s} & 0 & 0 \\ 0 & e^{-\frac{R_s}{L_s}T_s} & 0 \\ 0 & 0 & e^{-\frac{R_f^*}{L_f}T_s} \end{bmatrix}$$

$$\mathbf{B} = \begin{bmatrix} \frac{1-e^{-\frac{R_s}{L_s}T_s}}{R_s} & 0 & 3\frac{x_f^2}{n_s}\frac{1-e^{-\frac{R_f^*}{L_f}T_s}}{R_f^*}\cos\left(\frac{\phi}{2}\right) \\ 0 & \frac{1-e^{-\frac{R_s}{L_s}T_s}}{R_s} & -3\frac{x_f^2}{n_s}\frac{1-e^{-\frac{R_f^*}{L_f}T_s}}{R_f^*}\sin\left(\frac{\phi}{2}\right) \\ \frac{\lambda_{pm}}{L_s} & 0 & 0 \\ 0 & \frac{\lambda_{pm}}{L_s} & 0 \end{bmatrix}^T$$

$$\mathbf{C} = \begin{bmatrix} 1 & 0 & \frac{2}{3n_s}\cos\left(\frac{\phi}{2}\right) \\ 0 & 1 & -\frac{2}{3n_s}\sin\left(\frac{\phi}{2}\right) \end{bmatrix}. \qquad (8)$$

As the diagnostic algorithm presented in [6] provides updated parameters in matrices $\mathbf{A}$, $\mathbf{B}$, and $\mathbf{C}$ in each step, the matrices

are considered time-varying, indicated by the lower index k: $\mathbf{A}_k$, $\mathbf{B}_k$, and $\mathbf{C}_k$. Inputs $v_\alpha(k,k-1)$ and $v_\beta(k,k-1)$ in (6) were previously calculated in [6] by integrating the exponentially damped sine and cosine functions between steps $(k-1)T_s$ and kT_s, as follows:

$$\begin{bmatrix} v_\alpha(k,k-1) \\ v_\beta(k,k-1) \end{bmatrix} = \begin{bmatrix} -\cos\big(\theta_e(k)\big) & \sin\big(\theta_e(k)\big) \\ -\sin\big(\theta_e(k)\big) & -\cos\big(\theta_e(k)\big) \end{bmatrix} \begin{bmatrix} \frac{\bar{\omega}_e^2}{\frac{R_s^2}{L_s^2}+\bar{\omega}_e^2} \\ \frac{\bar{\omega}_e\frac{R_s}{L_s}}{\frac{R_s^2}{L_s^2}+\bar{\omega}_e^2} \end{bmatrix}$$

$$+ e^{-\frac{R_s}{L_s}T_s} \begin{bmatrix} \cos\big(\theta_e(k-1)\big) & -\sin\big(\theta_e(k-1)\big) \\ \sin\big(\theta_e(k-1)\big) & \cos\big(\theta_e(k-1)\big) \end{bmatrix} \begin{bmatrix} \frac{\bar{\omega}_e^2}{\frac{R_s^2}{L_s^2}+\bar{\omega}_e^2} \\ \frac{\bar{\omega}_e\frac{R_s}{L_s}}{\frac{R_s^2}{L_s^2}+\bar{\omega}_e^2} \end{bmatrix}. \qquad (9)$$

III. Monitoring the Hidden States

Kalman filtering algorithm presented in [11] was adopted to the specialized discrete-time model described above. The utilized algorithm's version recognizes three steps:

1) Data-updating steps:

$$\mathbf{K} = \mathbf{P}_{k|k-1}\mathbf{C}_k^T \big(\mathbf{R} + \mathbf{C}_k\mathbf{P}_{k|k-1}\mathbf{C}_k^T\big)^{-1}$$
$$\hat{\mathbf{e}}_{k|k-1} = \mathbf{y}(k) - \mathbf{C}_k\hat{\mathbf{x}}_{k|k-1}$$
$$\hat{\mathbf{x}}_{k|k} = \hat{\mathbf{x}}_{k|k-1} + \mathbf{K}\hat{\mathbf{e}}_{k|k-1}$$
$$\mathbf{P}_{k|k} = (\mathbf{I} - \mathbf{K}\mathbf{C}_k)\mathbf{P}_{k|k-1}(\mathbf{I} - \mathbf{K}\mathbf{C}_k)^T + \mathbf{K}\mathbf{R}\mathbf{K}^T. \qquad (10)$$

2) Forgetting factor adjustment:

$$\hat{\mathbf{e}}_{k|k} = \mathbf{y}(k) - \mathbf{C}_k\hat{\mathbf{x}}_{k|k}$$
$$\mathbf{F} = \mathbf{A}_k - \mathbf{S}\mathbf{R}^{-1}\mathbf{C}_k$$
$$\Xi = \frac{\hat{\mathbf{e}}_{k|k}^T\mathbf{R}^{-1}\mathbf{C}_k\mathbf{P}_{k|k-1}\mathbf{C}_k^T\mathbf{R}^{-1}\hat{\mathbf{e}}_{k|k} - \mathrm{tr}(\mathbf{C}_k\mathbf{K}) + 3}{\lambda_{k|k-1}}$$
$$+ \ln\left(\frac{|\mathbf{F}\mathbf{P}_{k|k}\mathbf{F}^T||\mathbf{R} + \mathbf{C}_k\mathbf{P}_{k|k-1}\mathbf{C}_k^T||\mathbf{R}|^{-1}}{|\mathbf{F}\mathbf{P}_{k|k}\mathbf{F}^T + \mathbf{Q} - \mathbf{S}\mathbf{R}^{-1}\mathbf{S}^T|}\right)$$
$$+ 3\ln(\lambda_{k|k-1})$$
$$\lambda_{k+1|k} = \frac{1}{\max\{\Xi/3, 1\}}. \qquad (11)$$

3) Time-updating steps:

$$\hat{\mathbf{x}}_{k+1|k} = \mathbf{A}_k\hat{\mathbf{x}}_{k|k} + \mathbf{B}_k\mathbf{u}(k) + \mathbf{S}\mathbf{R}^{-1}\hat{\mathbf{e}}_{k|k}$$
$$\mathbf{P}_{k+1|k} = \big(\mathbf{F}\mathbf{P}_{k|k}\mathbf{F}^T + \mathbf{Q} - \mathbf{S}\mathbf{R}^{-1}\mathbf{S}^T\big)\lambda_{k+1|k}^{-1}. \qquad (12)$$

In (10) - (12), $\mathbf{I}^{3\times3}$ stands for the identity matrix, and the lower indexes $x|y$ refer to the inner steps of the utilized Kalman filter, where x represents the time-updating step, and y denotes the data-updating step. The characteristics propagated between the Kalman filter steps are estimates of the hidden states $\hat{\mathbf{x}}$, covariance matrix $\mathbf{P}$, and forgetting factor λ.

In our implementation, the measurement noise covariance matrix was set to $\mathbf{R} = 2 \cdot 10^{-5}\mathbf{I}^{2\times2}$, where $2 \cdot 10^{-5}$ was obtained by computing the variance of $\alpha - \beta$ currents at the setpoint of 0. The process noise covariance matrix was
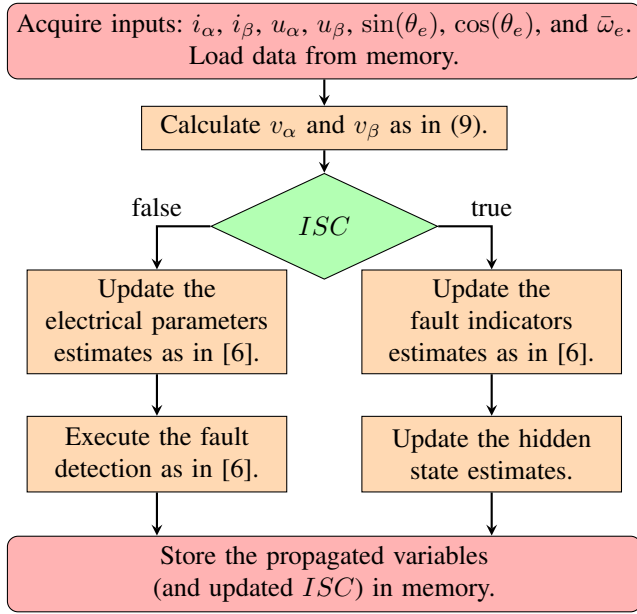
Fig. 2. One step in the extended fault diagnostic procedure.

Algorithm 1 Estimating the hidden states
1: **Initialization:**
2: Initialize the propagated covariance matrix $\mathbf{P} = \mathbf{I}^{3\times3}$, hidden states $\hat{\mathbf{x}} = \begin{bmatrix} 0 & 0 & 0 \end{bmatrix}^T$, and forgetting factor $\lambda = 1$. Set up initial delay τ in steps (utilized value: $\tau = 5$) and matrices $\mathbf{R}$, $\mathbf{Q}$, and $\mathbf{S}$.
3: **Hidden state estimation:**
4: **while** $ISC(k - \tau)$ **do**
5:     Update matrices $\mathbf{A}_k$, $\mathbf{B}_k$, and $\mathbf{C}_k$ as in (8) based on the current fault-related parameter estimates (electrical parameters are utilized as constants). Calculate $v_\alpha(k, k-1)$ and $v_\beta(k, k-1)$ as in (9) and form the input and output vectors $\mathbf{u}$ and $\mathbf{y}$ as in (6). Load the propagated characteristics $\mathbf{P}$, $\hat{\mathbf{x}}$, and λ from memory.
6:     Execute the data-updating steps (10), forgetting factor adjustment (11), and time-updating steps (12) in order. Store the updated characteristics $\mathbf{P}$, $\hat{\mathbf{x}}$, and λ in memory.
7: **end while**.

adjusted as $\mathbf{Q} = \mathrm{diag}(1 \cdot 10^{-4}, 1 \cdot 10^{-4}, 5 \cdot 10^{-3})$, where $\mathrm{diag}(x_1, x_2, ..., x_n) \in \mathbb{R}^{n \times n}$ represents the diagonal matrix. The implemented adaptive Kalman filter compensates for underrated process noise variance by real-time forgetting factor adjustments. Therefore, starting with lower values in $\mathbf{Q}$ and gradually increasing the variance to prevent the long-term forgetting factor fluctuations in a steady state helps to track the actual process noise. Since monitoring the fault current projection runs simultaneously with fault indicators estimation (and utilizes unsettled parameters), the process noise variance of $\tilde{i}_f$ is higher than that of $i_{\alpha,h}$ and $i_{\beta,h}$. The dependencies between the process and measurement noise components are then modeled using the covariance matrix $\mathbf{S}$ as follows:

$$\mathbf{S} = \begin{bmatrix} 2 \cdot 10^{-5} & 0 & 2 \cdot 10^{-5} \\ 0 & 2 \cdot 10^{-5} & 2 \cdot 10^{-5} \end{bmatrix}^T. \tag{13}$$

Even though, as yielded from (8), no direct dependency between i_β and $\tilde{i}_f$ is assumed if short circuits occur in phase a, we preserved the dependency between noise components to cover potential unmodeled nonlinearities. The covariances between measurement and process noises are then at the level of lower measurement noise variance.

Fig. 2 illustrates the integration of the developed approach for hidden state monitoring into the existing fault diagnostics framework presented in [6]. As shown in Fig. 2, the fault diagnostics cover two branches switched by the binary variable ISC, which indicates the detected presence of an interturn short circuit fault. Before a short circuit detection, the diagnostic algorithm learns the electrical parameters respecting the actual operating point and detects fault based on the rapid changes in the estimated parameters attributable to fault presence. After the fault is detected, the identified electrical parameters are utilized as constants, and fault location and severity are tracked. The estimator of hidden states then
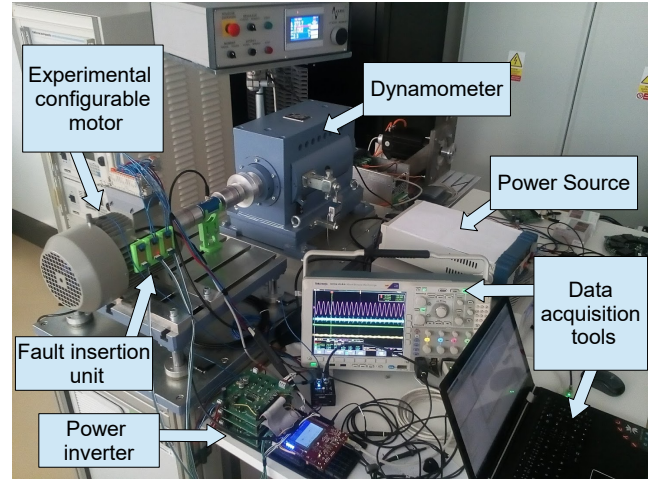

Fig. 3. The fault diagnostics testing setup.

relies on recursively updated fault-related parameters; thus, its performance is highly dependent on the settlement of these fault indicators. Therefore, it is recommended to delay the start of the state monitoring algorithm slightly to prevent the occurrence of undefined results. The hidden state monitoring algorithm reads Algorithm 1.

IV. VALIDATING THE HIDDEN STATE MONITORING

The monitoring was tested by using a vector-controlled 200 W machine (estimated $R_s = 0.515\,\Omega$, $L_s = 1.58$ mH, and $\lambda_{pm} = 9.88$ mWb). The windings of the utilized motor contain three coil segments in series ($n_p = 1$ and $n_s = 3$), each comprising 25 turns. The diagnostic algorithm (Fig. 2), triggered after calculating control action updates, is executed with a 10 kHz sampling frequency at an AURIX Application kit TC277, which controls an NXP three-phase low voltage power stage. In the three-core microcontroller TC277, the first core is dedicated to the control algorithm, the second integrates the diagnostic algorithm, and the third facilitates communication. The testing setup is depicted in Fig. 3.
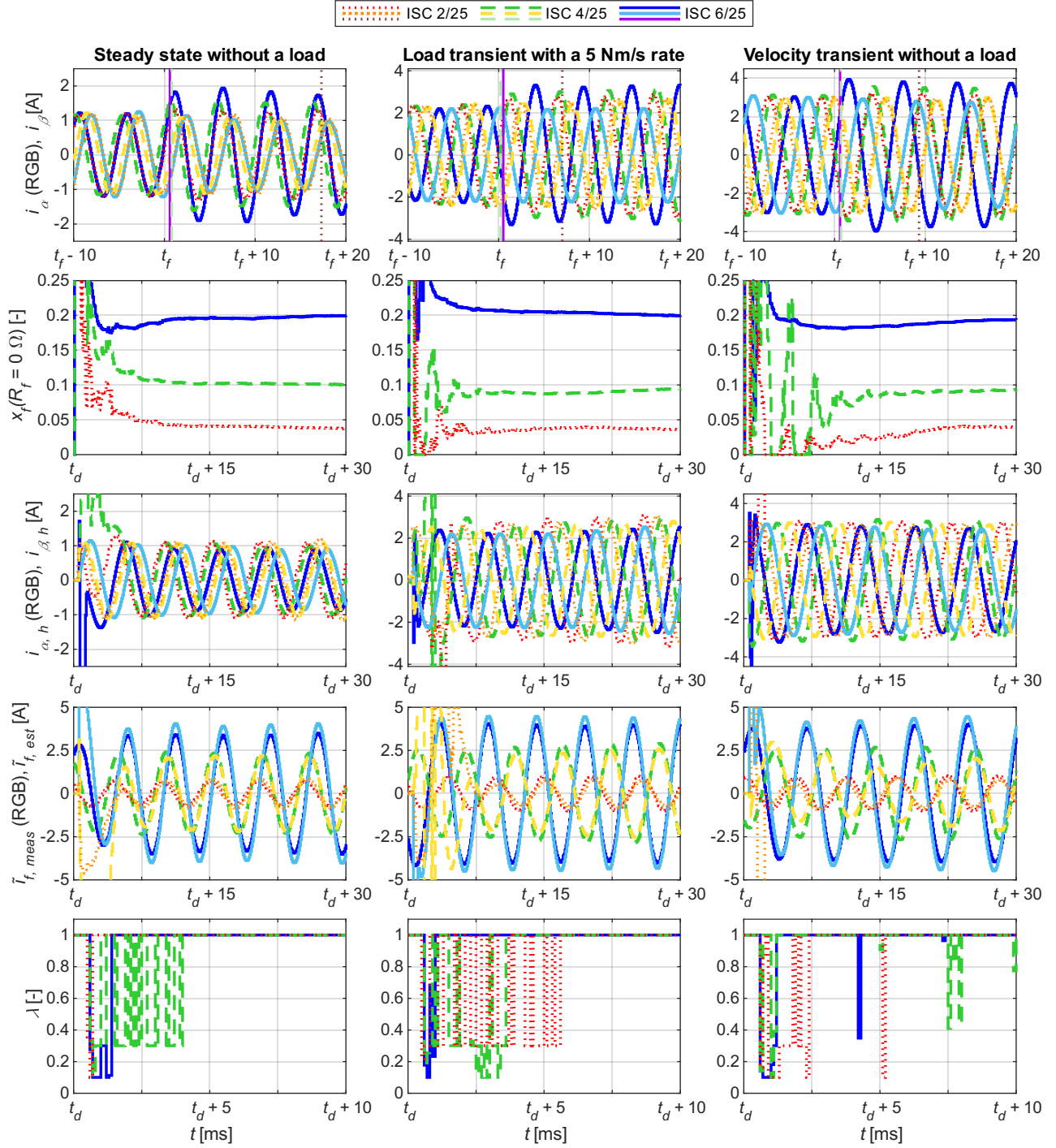
Fig. 4. Outcomes of hidden state monitoring experiments: measured $\alpha - \beta$ currents, estimated fault severity and hidden states, and variable forgetting factor.

As shown in Fig. 3, ISCs are emulated by the fault insertion unit, which contains an anti-series arrangement of two PSMNR90-50SLH MOSFET power transistors and an ACS709 current sensor for fault current measurement.

The validation included diverse fault severity values (2/25, 4/25, and 6/25) emulated in phase a and three distinct experiment types: Steady state without a load, Load transient with a 5 Nm/s rate change, and Velocity transient without a load. The outcomes of validation experiments are presented in Fig. 4. In the first scenario, the experimental motor was driven to

the angular velocity setpoint of 1200 rad/s without additional load exerted by a dynamometer, and ISCs were emulated after reaching the setpoint. In the second type of experiment, the machine, driven to the same velocity setpoint, was loaded by 0.25 Nm, and after settling the velocity, faults were connected in the load transient (rise to 0.75 Nm with a 5 Nm/s rate). In the last experimental case, no additional load was exerted, and ISCs were emulated in the velocity transient from 800 to 1200 rad/s close to 1100 rad/s.

In Fig. 4, faults occurring at the time t_f are detected at

Measured Time	Data preproc.	El. params. estimation	Fault detection	Fault. ind. estimation	Hid. state monitoring
Min [μs]	1.0	28.6	51.0	53.2	12.4
Average [μs]	1.2	29.8	52.7	54.8	12.9
Max [μs]	1.5	30.4	54.5	60.1	13.4

t_d, indicated by the vertical lines in the graphs displaying measured $\alpha - \beta$ currents. The accuracy of hidden state monitoring is then highly dependent on the estimated fault severity $x_f(R_f = 0\,\Omega)$ settlement. However, the forgetting factor λ adjustments help to suppress the uncertain information caused by varying fault-related parameters, and the hidden state estimates quickly converge to the actual values. As also seen in Fig. 4, $i_{\alpha,h}$ and $i_{\beta,h}$, reconstructed by the Kalman filter, track even the growing pattern caused by the load change, and estimated $\tilde{i}_{f,est}$ nearly corresponds to the measured values $\tilde{i}_{f,meas}$. The differences are most likely caused by assuming rounded values of fault severity 2/25, 4/25, and 6/25 in the calculation of $\tilde{i}_{f,meas}$. These values do not reflect different coil lengths and fault terminal attachment shifts, which can be up to ± 0.5 turns.

The computational requirements of the designed hidden state monitoring algorithm implemented at the AURIX Application kit TC277 were measured and compared with the execution times of other fault diagnostics parts (Fig. 2) presented in [6]. Table I compares the computational times of individual fault diagnostic algorithm parts. Regarding the information in Table I, the hidden state monitoring algorithm is the most efficient part of fault diagnostics (data preprocessing excluded). Overall diagnostic algorithm then uses one TC277 microcontroller core at 83 - 88 % before an ISC is detected, and the load decreases at 68 - 77 % after fault detection.

V. Conclusion

In this paper, the existing modular fault diagnostic algorithm was extended by hidden state monitoring. The solution relies on the adaptive Kalman filter and specialized discrete-time model. The monitoring algorithm utilizes parameters and fault indicators estimated for the actual operating point and functions even in the transient states. Furthermore, the diagnostics, including the monitoring method, are computationally efficient as they use only one core of the AURIX microcontroller at a maximum of 88 %. A comparison with the existing diagnostic algorithm was introduced in [6]. The extensions designed in this manuscript preserve all the advantages, which are further enhanced by hidden state monitoring, but also the disadvantage because the algorithm functions only if $L_d \approx L_q$.

References

[1] Y. Qi, E. Bostanci, V. Gurusamy and B. Akin, "A Comprehensive Analysis of Short-Circuit Current Behavior in PMSM Interturn Short-Circuit Faults," in IEEE Trans. Power Electron., vol. 33, no. 12, pp. 10784-10793, Dec. 2018, doi: 10.1109/TPEL.2018.2809668.

[2] S. Huang, A. Aggarwal, E. G. Strangas, B. Khoshoo, K. Li and F. Niu, "Mitigation of Interturn Short-Circuits in IPMSM by Using MTPCC Control Adaptive to Fault Severity," in IEEE Trans. Power Electron., vol. 37, no. 4, pp. 4685-4696, Apr. 2022, doi: 10.1109/TPEL.2021.3127538.

[3] F. Chen, J. Fan, W. Li, J. Fang, and S. Ding, "Mitigation of high-resistance connection in surface-mounted PMSM drive system based on model predictive current control," Results in Engineering, vol. 15. Elsevier BV, p. 100590, Sept. 2022. doi: 10.1016/j.rineng.2022.100590.

[4] J. Zhang, W. Zhan and M. Ehsani, "Fault-Tolerant Control of PMSM With Inter-Turn Short-Circuit Fault," in IEEE Trans. Energy Convers., vol. 34, no. 4, pp. 2267-2275, Dec. 2019, doi: 10.1109/TEC.2019.2936225.

[5] I. Jeong, B. J. Hyon and K. Nam, "Dynamic Modeling and Control for SPMSMs With Internal Turn Short Fault," in IEEE Trans. Power Electron., vol. 28, no. 7, pp. 3495-3508, July 2013, doi: 10.1109/TPEL.2012.2222049.

[6] L. Zezula, M. Kozovsky and P. Blaha, "Diagnostics of Interturn Short Circuits in PMSMs with Online Fault Indicators Estimation," in IEEE Trans. Ind. Electron., doi: 10.1109/TIE.2024.3363775.

[7] J. Dokoupil, M. Papež and P. Václavek, "Comparison of Kalman filters formulated as the statistics of the Normal-inverse-Wishart distribution," 2015 54th IEEE Conf. Decision Control, Osaka, Japan, 2015, pp. 5008-5013, doi: 10.1109/CDC.2015.7403002.

[8] J. Dokoupil and P. Václavek, "Regularized Estimation with Variable Exponential Forgetting," 2020 59th IEEE Conf. Decision Control, Jeju, Korea (South), 2020, pp. 312-318, doi: 10.1109/CDC42340.2020.9304385.

[9] L. Zezula, Fault relevance diagnostics of the PMSM under the inter-turn short circuit fault, Brno, 2022, 85 p. Master's thesis. Brno University of Technology, Faculty of Electrical Engineering and Communication, Department of Control and Instrumentation.

[10] L. Zezula and P. Blaha, "Discrete-Time Modeling of PMSM for Parametric Estimation and Model Predictive Control Tasks," in Proc. IECON 49th Annu. Conf. IEEE Ind. Electron. Soc., Singapore, Singapore, 2023, doi: 10.1109/IECON51785.2023.10312226.

[11] J. Dokoupil and P. Václavek, "Forgetting Factor Kalman Filter with Dependent Noise Processes," 2019 IEEE 58th IEEE Conf. Decision Control, Nice, France, 2019, pp. 1809-1815, doi: 10.1109/CDC40024.2019.9029683.

[12] L. Otava and L. Buchta, "Permanent magnet synchronous motor stator winding fault detection," in Proc. IECON 42nd Annu. Conf. IEEE Ind. Electron. Soc., Florence, Italy, 2016, pp. 1536-1541, doi: 10.1109/IECON.2016.7793941.

[13] S. -G. Ahn, B. -G. Park, R. -Y. Kim and D. -S. Hyun, "Fault diagnosis for open-phase faults of permanent magnet synchronous motor drives using Extended Kalman Filter," in Proc. IECON 36th Annu. Conf. IEEE Ind. Electron. Soc., Glendale, AZ, USA, 2010, pp. 835-840, doi: 10.1109/IECON.2010.5675176.

[14] B. Aubert, J. Régnier, S. Caux and D. Alejo, "Kalman-Filter-Based Indicator for Online Interturn Short Circuits Detection in Permanent-Magnet Synchronous Generators," in IEEE Trans. Ind. Electron., vol. 62, no. 3, pp. 1921-1930, Mar. 2015, doi: 10.1109/TIE.2014.2348934.

[15] V. Nguyen, D. Wang, J. Seshadrinath, S. Nadarajan and V. Vaiyapuri, "Fault severity estimation using nonlinear Kalman filter for induction motors under inter-turn fault," in Proc. IECON 42nd Annu. Conf. IEEE Ind. Electron. Soc., Florence, Italy, 2016, pp. 1488-1493, doi: 10.1109/IECON.2016.7792962.

[16] M. Romdhane, M. Naoui, and A. Mansouri, "PMSM Inter-Turn Short Circuit Fault Detection Using the Fuzzy-Extended Kalman Filter in Electric Vehicles," Electronics, vol. 12, no. 18. MDPI AG, p. 3758, Sep. 06, 2023. doi: 10.3390/electronics12183758.

[17] C. Li, K. Baruti and B. Akin, "Online Short-Circuit Current Estimation of Permanent Magnet Motors," in IEEE Trans. Power Electron., vol. 37, no. 12, pp. 15554-15570, Dec. 2022, doi: 10.1109/TPEL.2022.3195487.

[18] Y. Qi, M. Zafarani, V. Gurusamy and B. Akin, "Advanced Severity Monitoring of Interturn Short Circuit Faults in PMSMs," in IEEE Transactions on Transportation Electrification, vol. 5, no. 2, pp. 395-404, June 2019, doi: 10.1109/TTE.2019.2913357.

[19] R. T. Meyer, R. A. DeCarlo, S. C. Johnson and S. Pekarek, "Short-Circuit Fault Detection Observer Design in a PMSM," in IEEE Transactions on Aerospace and Electronic Systems, vol. 54, no. 6, pp. 3004-3017, Dec. 2018, doi: 10.1109/TAES.2018.2836618.

[20] W. Li, J. Hang, S. Ding and Q. Wang, "Common Predictive Model for PMSM Drives With Interturn Fault Considering Torque Ripple Suppression," in IEEE Transactions on Transportation Electrification, vol. 9, no. 3, pp. 4071-4079, Sept. 2023, doi: 10.1109/TTE.2022.3232820.